



Contents lists available at SciVerse ScienceDirect

## Journal of Constructional Steel Research



## Overall buckling behavior of all-steel buckling restrained braces

N. Hoveidae<sup>a,b</sup>, B. Rafezy<sup>a,\*</sup><sup>a</sup> Civil engineering Faculty, Sahand University of Technology, Sahand, Tabriz, East Azarbayjan, Iran<sup>b</sup> Ecole Polytechnique de Montreal, Quebec, Canada

## ARTICLE INFO

## Article history:

Received 26 November 2011

Accepted 24 July 2012

Available online xxxx

## Keywords:

All-steel buckling restrained brace

Global buckling

Finite element analysis

Cyclic loading

## ABSTRACT

One of the key requirements for the desirable mechanical behavior of buckling restrained braces (BRBs) under severe earthquake loading is to prevent global buckling until the brace member reaches sufficient plastic deformation and ductility. This paper presents finite element analysis results of the proposed all-steel buckling restrained braces. The proposed BRBs have identical core sections but different buckling restraining mechanisms (BRMs). The objective of the analysis is to conduct a parametric study of BRBs with different amounts of gap (between the core and the BRM) and initial imperfections to investigate the global buckling behavior of the brace. The results of the analysis showed that BRM flexural stiffness could significantly affect the global buckling behavior of a brace, regardless of the size of the gap. In addition, a minimum ratio of the Euler buckling load of the restraining member to the yield strength of the core,  $P_e/P_y$ , is suggested for design purposes. This ratio is the principal parameter that controls the global buckling of BRBs.

© 2012 Elsevier Ltd. All rights reserved.

## 1. Introduction

Buckling restrained braced frames (BRBFs) for seismic load resistance have been widely used in recent years. A BRBF differs from a conventionally braced frame because it yields under both tension and compression without significant buckling. Most buckling restrained brace (BRB) members currently available are built by inserting a steel plate into a steel tube filled with mortar or concrete. The steel plate is restrained laterally by the mortar or the steel tube and can yield in compression as well as tension, which results in comparable yield resistance and ductility, as well as a stable hysteretic behavior in BRBs. A large body of knowledge exists regarding conventional BRBs' performance. Black et al. performed component testing of BRBs and modeled a hysteretic curve to compare the test results and found that the hysteretic curve of a BRB is stable, symmetrical, and ample [1]. Inoue et al. introduced buckling restrained braces as hysteretic dampers to enhance the seismic response of building structures [2]. As shown in Fig. 1, a typical BRB member consists of a steel core, a buckling restraining mechanism (BRM), and a separation gap or unbonding agent, allowing independent axial deformation of the inner core relative to the BRM. Numerous researchers have conducted experiments and numerical analyses on BRBs for its incorporation into seismic force resisting systems. Qiang investigated the use of BRBs in practical applications for buildings in Asia [3]. Clerk et al. suggested a design procedure for buildings incorporating BRBs [4]. Sabelli et al. reported seismic demands on BRBs through a seismic response analysis of BRB frames [5], and Fahnestock et al. conducted a

numerical analysis and pseudodynamic experiments of large-scale BRB frames in the US [6].

The local buckling behavior of BRBs has been studied by Takeuchi et al. [7]. The effective buckling load of BRBs considering the stiffness of the end connection was recently studied by Tembata et al. [8] and Kinoshita et al. [9]. Previous studies have demonstrated the potential of manufacturing BRB systems made entirely of steel, called all-steel BRBs [10]. In a common all-steel BRB, the steel inner core is sandwiched between buckling restraining mechanisms made entirely of steel components, thus avoiding the cost of mortar needed in conventional BRBs. This eliminates the fabrication steps associated with pouring and curing the mortar or concrete, significantly reducing manufacturing time and costs. In addition, such a BRB can be easily disassembled for inspection after an earthquake. Experimental and analytical studies on the deformation performance and dynamic response of BRBs have been performed by Kato et al. [11], Watanabe et al. [12], and Usami et al. [13]. The restraining member proposed previously was a mortar-filled steel section, which made an extremely rigid member. In such types of BRBs, the brace member and the BRM were integrated, and overall buckling did not occur. However, in all-steel BRBs, which are considered to be a new generation of BRBs, the brace system is completely made of steel, and the BRM system is lighter in comparison with conventional BRBs, which leads to a high potential for brace overall buckling caused by the low rigidity and stiffness of the BRM. The hysteretic behavior of all-steel BRBs was experimentally investigated by Tremblay et al. [10]. An experimental study on the hysteretic behavior of all-steel BRBs was also conducted by Eryasar et al. [14].

The following characteristics are considered necessary for the safe performance of BRBs: 1) the prevention of overall buckling, 2) the prevention of core local buckling, 3) the prevention of low cycle

\* Corresponding author. Tel.: +98 9143016119.

E-mail addresses: Hoveidae@gmail.com, Nader.Hoveidae@polymtl.ca (N. Hoveidae), Rafezyb@sut.ac.ir (B. Rafezy).

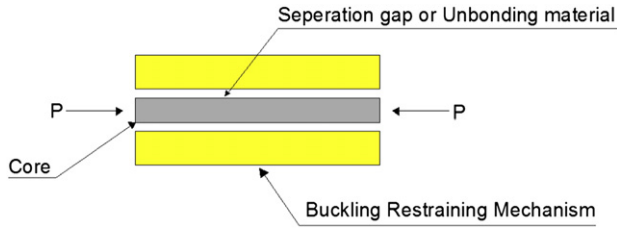


Fig. 1. Components of a BRB [10].

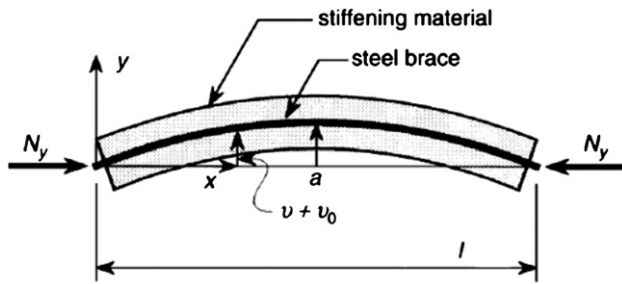


Fig. 2. Force and deformation of a BRB [20].

fatigue of the brace member, and 4) high strength of the joint parts and connections. In this paper, the first characteristic (i.e., overall buckling behavior) is examined further.

Assume a BRB member with initial deflection under compression. When the inner core with initial inherent imperfection deflects under compression, it comes into contact with the BRM, the contact forces increase the out-of-plane deformation of the entire BRB and strength deterioration occurs before the brace member reaches the target displacement if the rigidity and strength of the BRM are insufficient. According to the AISC 2010 guidelines for qualifying cyclic tests of BRBs [15], a BRB should sustain axial deformations of up to  $\Delta_{bm}$ , where  $\Delta_{bm}$  is the brace axial deformation corresponding to the design story drift. The buckling restraining mechanism should have enough strength and rigidity to prevent overall buckling of the brace during axial deformation. Therefore, to obtain the hysteretic characteristic on the compression side similar to that on the tension side and to mitigate pinching, it becomes necessary to avoid overall buckling (i.e., flexural buckling). The results of the first studies on overall buckling behavior of BRBs conducted by Watanabe et al. revealed that the ratio of the Euler buckling load of the restraining member to the yield strength of the core,  $P_e/P_y$ , is the factor that most accurately determines the capacity to control brace global buckling [16]. These authors concluded that if the ratio of the Euler buckling load of the BRM to the yield load of the inner

core,  $P_e/P_y$ , is less than one, the brace member will experience overall buckling during cyclic loading of the braced frame. However, a  $P_e/P_y$  ratio of 1.5 was proposed for design purposes in the studies mentioned. The criterion  $P_e/P_y \geq 1$  has a theoretical basis [1] and has been verified by Iwata et al. through experimental testing [17]. Similar experimental studies were conducted by Usami et al. [13] on all-steel BRBs, and a safety factor of  $\lambda_f = P_{\max}/P_y$  was proposed where  $P_{\max}$  and  $P_y$  denote the maximum compression force in the brace member and the core yielding capacity, respectively. The safety factor is illustrated as follows:

$$\gamma_f = \frac{1}{\left(\frac{P_y}{P_e}\right) + \left(\frac{P_y}{M_y}\right) \cdot (a + d + e)} \quad (1)$$

where  $a$ ,  $d$ , and  $e$  are the initial deflection, gap amplitude, and the eccentricity of loading, respectively. Test results showed that if the value of safety factor  $\gamma_f$  was greater than three, overall buckling of BRB would not occur.

The finite element analysis method was recently used with success to predict the buckling response of the core plates in BRB members with tubes filled with mortar [18]. Subsequent finite element analysis studies have been conducted by Tremblay et al. to investigate the core buckling behavior in all-steel BRBs [19]. The studies mentioned above also provided a description of the complex interaction that develops between the brace core and BRM. Outward forces induced by the contact forces were found to be resisted in flexure by the BRM components located on each side of the core. In addition, the contact forces resulted in longitudinal frictional forces that induced axial compression loads in the BRM. The representative  $P_e/P_y$  ratio used in these studies was 3.5, and the test results showed that the encasing strength was adequate to prevent global buckling of the brace.

This paper investigates the finite element analysis studies of overall buckling behavior of all-steel BRBs regarding the effect of the gap amplitude between the core and BRM and the initial imperfection of an entire BRB member. Finally, the overall buckling prevention condition of the proposed BRBs is suggested for design purposes.

## 2. Overall buckling criterion of BRBs

An analysis of the elastic buckling of a composite brace composed of a steel core encased by a restrainer showed that the critical load of the entire brace member under compression could be found by solving an equilibrium equation as follows [20]:

$$E_B I_B \cdot \frac{d^2 v}{dx^2} + (v + v_0) N_{\max} = 0 \quad (2)$$

in which  $E_B I_B$  is the flexural stiffness of the BRM,  $N_y$  represents the brace yielding load, and  $v$  and  $v_0$  denote the transverse and the initial

**Table 1**  
BRB specimen properties.

No.	Model name	BRM dimensions (mm)	Core dimensions (mm)	$A_c$ (mm <sup>2</sup> )	gap (mm)	$I_r$ (mm <sup>4</sup> )	$P_e$ (KN)	$P_{yc}$ (KN)
1	S1g <sub>0.5</sub>	UNP 50 + 2 face plates (45×5)	Plate 100×10	1000	0.5	850,000	419	370
2	S2g <sub>0.5</sub>	UNP 65 + 2 face plate (37.5×5)	Plate 100×10	1000	0.5	1,160,000	571	370
3	S3g <sub>0.5</sub>	BOX (50×50×3) + 2 face plate (45×5)	Plate 100×10	1000	0.5	1,530,000	752	370
4	S4g <sub>0.5</sub>	BOX (50×50×4) + 2 face plate (45×5)	Plate 100×10	1000	0.5	1,950,000	963	370
5	S1g <sub>2</sub>	UNP 50 + 2 face plate (45×5)	Plate 100×10	1000	2.0	960,000	475	370
6	S2g <sub>2</sub>	UNP 65 + 2 face plate (37.5×5)	Plate 100×10	1000	2.0	1,300,000	639	370
7	S3g <sub>2</sub>	BOX (50×50×3) + 2 face plate (45×5)	Plate 100×10	1000	2.0	1,660,000	816	370
8	S4g <sub>2</sub>	BOX (50×50×4) + 2 face plate (45×5)	Plate 100×10	1000	2.0	2,110,000	1042	370
9	S5g <sub>2</sub>	PL (35×10) + 2 face plate (45×5)	Plate 100×10	1000	2.0	820,000	406	370
10	S1g <sub>0</sub>	UNP 50 + 2 face plate (45×5)	Plate 100×10	1000	–	810,000	401	370
11	S2g <sub>0</sub>	UNP 65 + 2 face plate (37.5×5)	Plate 100×10	1000	–	1,120,000	551	370
12	S3g <sub>0</sub>	BOX (50×50×3) + 2 face plate (45×5)	Plate 100×10	1000	–	1,480,000	732	370
13	S4g <sub>0</sub>	BOX (50×50×4) + 2 face plate (45×5)	Plate 100×10	1000	–	1,900,000	937	370

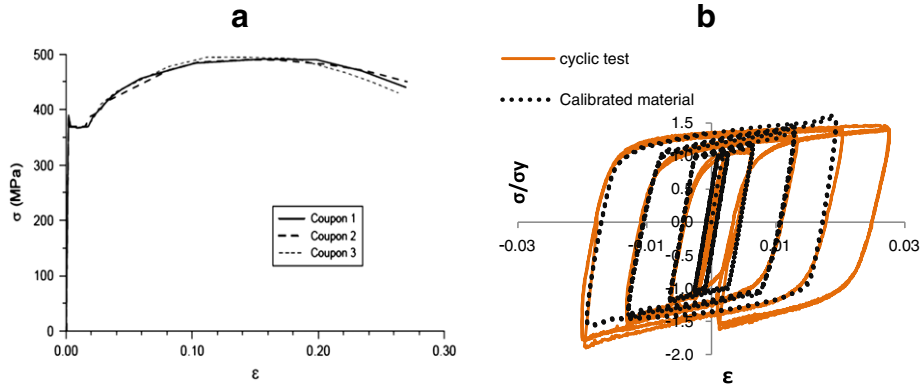


Fig. 3. a) Stress–strain curve resulted from the test [10], b) Calibrated hysteretic response of the steel material [19].

deflection of the brace member, respectively, as shown in Fig. 2. The initial deflection of the brace is assumed to be expressed by a sinusoidal curve as follows:

$$v_0 = a \sin \frac{\pi x}{L} \quad (3)$$

where  $a$  is the initial deflection of the brace at the center, and  $N$  is the brace axial load, which is replaced with  $P$  in the following equations. Solving the equilibrium Eq. (2) results in the following:

$$v + v_0 = \frac{a}{1 - \frac{P_{\max}}{P_e}} \sin \frac{\pi x}{L}. \quad (4)$$

The bending moment at the center of BRM can be written as follows [20]:

$$M_c = \frac{P_{\max} \cdot a}{1 - \frac{P_{\max}}{P_e}} \quad (5)$$

where  $P_{\max}$  is the maximum axial force of the brace. Assuming that  $P_{\max}$  is equal to the  $P_y$  (i.e., yield load of the core) and considering that the buckling of the BRB occurs when the maximum stress in the outermost fiber of the BRM reaches the yield stress, the requirement for stiffness and strength of the steel tube (BRM) can be obtained as follows:

$$\frac{P_e}{P_y} \geq 1 + \frac{\pi^2 E_B \cdot a \cdot D}{2 \sigma_y \cdot L_B^2} \quad (6)$$

in which  $L_B$ ,  $\sigma_y$ , and  $D$  denote the length, the yield stress of the steel tube, and the depth of the restraining member section, respectively. This is the first formula that successfully expresses strength and stiffness requirements as paired in the design of BRBs. In this formula, the

effect of gap amplitude,  $g$ , has not been considered in the calculation of the moment at the center of the BRM. Therefore, in this paper, this parameter is involved in Eq. (6). Thus, Eq. (6) can be modified as follows:

$$\frac{P_e}{P_y} \geq 1 + \frac{\pi^2 E_B \cdot (a + g) \cdot D}{2 \sigma_y \cdot L_B^2} = \beta \quad (7)$$

where  $L_B$  is the length of the core and BRM (equal together), and  $D$  is the depth of the BRM section. Eq. (7) indicates that overall buckling of the brace will not occur if the ratio  $P_e/P_y$  is greater than the parameter  $\beta$ , which is calculated based on the geometric characteristics and material characteristics of the brace member.

### 3. Finite element analysis

To provide a numerical understanding of the cyclic behavior and buckling load of all-steel BRBs, an analysis using the finite element analysis method was conducted on 13 BRB specimens. A tri-dimensional representation of the brace specimens was developed to properly capture the observed behavior. The models included the core plates, and the BRM components consist of tubes, guide plates, filler plates, and end stiffeners.

#### 3.1. Description of the models

Numerical studies have been conducted on 13 proposed all-steel BRBs. Table 1 represents the details and specifications of the models where the first column shows the specimen code in the form  $S_i g_i$ , in which indexes  $i$  and  $g$  represent the model number and gap amplitude at the interface, respectively. All models consisted of a constant  $100 \times 10 \text{ mm}^2$  core plate with various cross sections for BRM members,

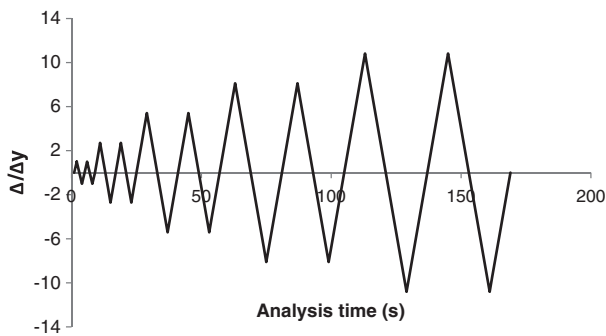


Fig. 4. Loading protocol of the BRB models.

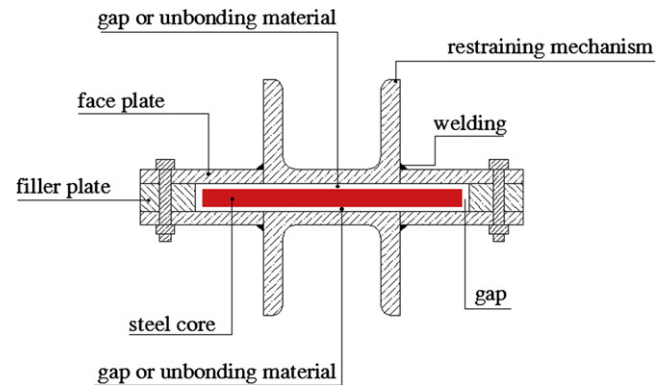


Fig. 5. Typical cross section of proposed BRBs.

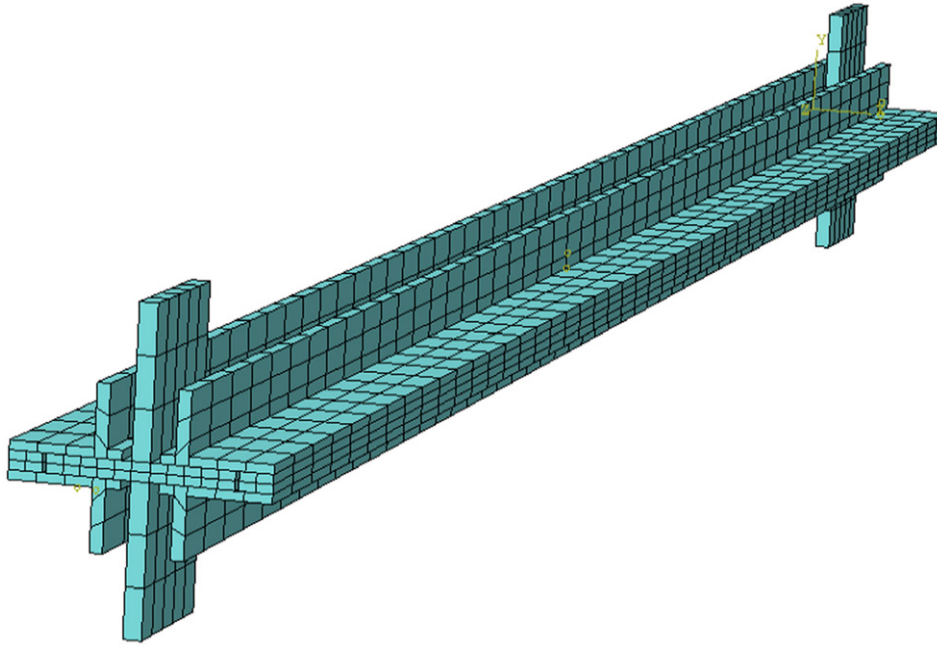


Fig. 6. Finite element model of a proposed BRB.

as shown in Table 1. Therefore, the yield strength of the core was kept constant when the stiffness and strength of the BRMs were altered. In addition, the effect of the generation of a gap between the core and the BRM was considered in the analysis. The total length of the BRBs,  $L$ , was assumed to be 2000 mm. The core plate's yield load,  $P_y$ , was calculated by multiplying the yield stress by the cross-sectional area, and the buckling load of the BRM,  $P_e$ , was calculated from the Euler buckling load formula.

The core plate and BRM were modeled using 8-node C3D8R linear brick elements with reduced integration. Large displacement static cyclic analysis was performed using the ABAQUS 6.9.3 [21] general-purpose finite element program. The full Newton–Raphson method was considered for solving nonlinear equations in the analysis. Automatic stabilization factor using a damping coefficient of  $2.0 \times 10^{-4}$  was specified to simplify the convergence. A nonlinear static problem can be unstable. Such instabilities may be of a geometrical nature, such as buckling, or of a material nature, such as material softening. ABAQUS provides an automatic mechanism for stabilizing unstable quasi-static problems through the automatic addition of volume-proportional damping to the model. The adaptive automatic stabilization scheme, in which the damping factor can vary spatially and with time, provides an effective alternative approach. In this case the damping factor is controlled by the convergence history and the ratio of the energy dissipated by viscous damping to the total strain energy. If the convergence behavior is problematic because of instabilities or rigid body modes, ABAQUS automatically increases the damping factor. In this study, the default accuracy tolerance of 0.05 was assumed for adaptive stabilization. Also, maximum and minimum increment sizes of 0.25 and  $1 \times 10^{-6}$ , respectively, were specified in the analysis.

The face and filler plates were connected together using a tie interaction type to simulate a continuous welded connection. The core plate was expected to undergo large plastic deformations and higher mode buckling with pronounced curvature. Therefore, a solid element with a refined mesh was adopted with five elements across the plate and two over the thickness for the core plate. A coarser mesh was used for the BRM because most of this component was expected to remain elastic. Contact properties with tangential Coulomb frictional behaviors were assumed between the core and the BRM elements. For this purpose, a surface to surface contact property with an approximate automatic stabilization factor of  $1 \times 10^{-4}$  was considered to achieve a better convergence. However, the magnitude of

the stabilizing factor was dependent on the model properties and it was altered whenever the analysis faced convergence difficulties. Contact stabilization is based on viscous damping opposing relative motion between nearby surfaces without degrading the accuracy of the results. Tangential contact behavior with a frictional coefficient of 0.1 was adopted to simulate a greasy smooth interface between the steel material of the core plate and the BRM. The same frictional coefficient was considered in the similar analysis conducted by Chou et al. [22]. In addition, a friction coefficient of 0.075 was adopted between the unbonding agent and the encasing in the analysis performed on BRBs by Usami et al. [23].

The authors of this paper strongly believe that the magnitude of the contact frictional coefficient between the core and the encasing considerably affects the overall and local buckling response of BRBs. The authors have conducted extensive analyses to investigate the effect of frictional response in BRBs. The results of those analyses showed that the axial force transmitted into the BRM increases with the increase in the amount of frictional coefficient between the contact surfaces. The intensified axial forces due to frictional shear forces at the interface result in excessive bending moments in the BRM because of P- $\Delta$  effects. Therefore, the overall buckling load of the entire BRB may change by involving the friction effects. Similar results were reported by Korzekwa et al. [19]. In this paper, the authors did not put emphasis on this phenomenon. Therefore, a smooth greasy contact surface between the core and the encasing was adopted. However, a friction coefficient of 0.3 may be adopted for rough and dry surfaces between the core and BRM as regarded in the research by Korzekwa et al. [19].

A hard contact rule was assumed for the normal direction which minimized the penetration of the core and BRM surfaces. The contact model allowed for the separation of the core plate from the BRM elements, which enabled higher mode buckling of the core plate. The core plate and the BRM components were made of steel with a yield stress of  $F_y = 370$  MPa. A Young modulus of 200 GPa and a Poisson ratio of 0.3 were assumed for the core plate and the BRM components. A nonlinear combined isotropic-kinematic hardening rule was employed to reproduce the inelastic material property and therefore an accurate cyclic behavior. The selection and calibration of steel material properties and the hardening parameters were based on Coupon and cyclic test results conducted by Tremblay et al. [10] and further analytical studies by Korzekwa et al. [19]. Based on those



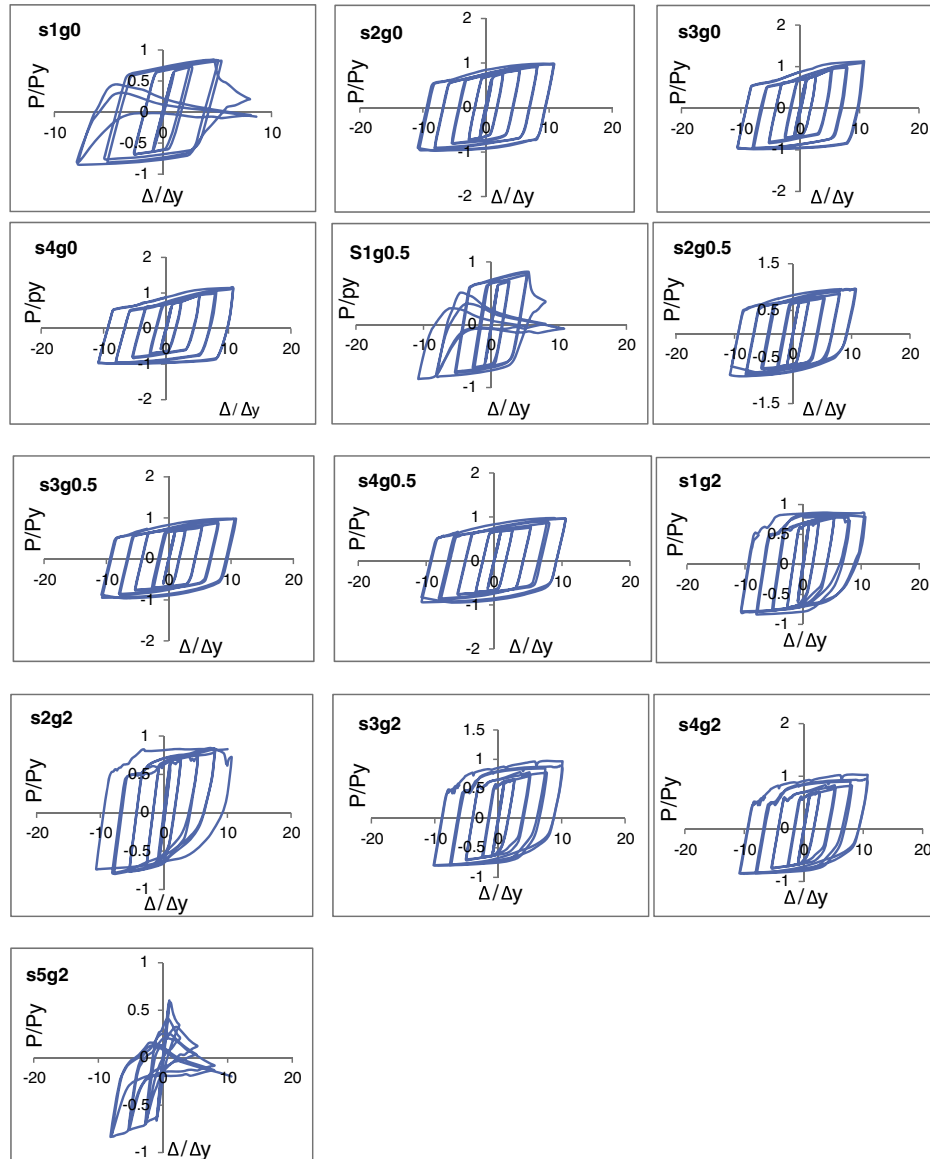


Fig. 7. Hysteretic responses of the proposed BRBs (compression is positive).

studies, the initial kinematic hardening modulus  $C$  and the rate factor  $\gamma$  were set to 8 GPa and 75, respectively [19]. For isotropic hardening, a maximum change in yield stress of  $Q_{\infty} = 110$  MPa and a rate factor of  $b = 4$  were adopted. Fig. 3a and b represent the stress–strain curve of the steel material resulting from the tests and the calibrated cyclic response based on the combined hardening model, respectively [10,19].

An initial geometric imperfection of 2 mm (i.e.,  $L/1000$ ) was considered in both the core plate and the BRM in all models. There are several methods used to introduce the geometric imperfection into a model such as perturbation of the geometry based on the first mode buckling pattern or defining an imperfection based on the deformed geometry of a previous static analysis. In this paper, the latter method was used to apply the imperfection. A pre-defined linear static analysis was performed to specify the imperfection in the brace member before the nonlinear cyclic analysis. For this purpose, a surface load was applied to the core and the BRM to reach the required displacement (i.e. 2 mm) at the brace center. Subsequently, the nonlinear cyclic analysis was continued at the end of the first step starting from the compressive loading at the core end.

Three types of interfaces between the core plate and BRM were considered in the models. In the first case, a direct contact of the core plate with the BRM was implemented, and in the second and third cases, gap amplitudes of 0.5 and 2 mm, respectively, were provided through the core thickness. In addition, the constant gap amplitude of 2 mm was provided through the core width in all models. Such a gap was used to accommodate the free expansion of the inner core under axial loads. The axial deformation was blocked at one end of bracing with a pinned connection. Axial displacements were imposed at the other end following the cyclic quasi static protocol suggested by AISC seismic provisions for BRBs [15] as follows: 2 cycles at  $\pm \Delta_y$ , 2 cycles at  $\pm 0.5\Delta_{bm}$ , 2 cycles at  $\pm \Delta_{bm}$ , 2 cycles at  $\pm 1.5\Delta_{bm}$ , and 2 cycles at  $\pm 2\Delta_{bm}$ , where  $\Delta_y$  is the displacement that corresponds to the yielding of the core, and  $\Delta_{bm}$  is the axial deformation of the brace corresponding to the design story drift [15]. Based on the previous studies by Tremblay et al. [10], the peak strain amplitude in full-length core braces typically falls in the range of 0.01 to 0.02 for common structural applications, and peak deformation in the majority of past test programs have been limited to that range [16]. In this study,  $\Delta_{bm}$  was set to 20 mm, which corresponds to the axial strain of 1% in the core, and the core yielding displacement,

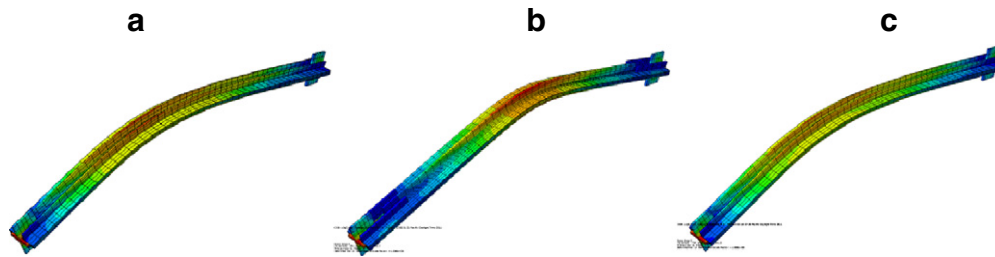


Fig. 8. Global buckling of BRBs, a) model  $S_{1g0}$ , b) model  $S_{5g2}$ , and c) model  $S_{1g0.5}$ .

$\Delta_y$ , was calculated as 3.7 mm based on the material characteristics. Hence, the ultimate axial displacement demand of the brace during cyclic loading was determined as  $2\Delta_{pm} = 40$  mm (i.e.  $\approx 11\Delta_y$ ), which corresponds to a core strain of 2%. Therefore, the adopted value for the peak strain demand of the core seems reasonable. Fig. 4 shows the loading protocol used in the analyses. A typical cross section of the proposed BRB members and its finite element representation are shown in Figs. 5 and 6, respectively.

#### 4. Results and discussions

Hysteretic responses in all of the BRB models are well predicted by the finite element model in both elastic and nonlinear ranges. Fig. 7 illustrates the normalized hysteretic responses of the braces in which the abscissa and ordinate represent the core normalized axial deformation and axial force, respectively.

Axial force–displacement curves of the BRB models are captured from a point at the brace end. This point is located in a region that essentially remains elastic, since stiffener plates are provided in this region to prevent local buckling at the brace end. Therefore, the captured force–displacement relation may not be a representation of the true stress distribution of the core during cyclic loading, although the curves properly describe the deterioration in strength caused by the global or local buckling of the brace. The axial force–deformation curves shown in Fig. 7 indicate the sudden deterioration in strength and overall buckling in the models  $S_{1g0.5}$ ,  $S_{5g2}$ , and  $S_{1g0}$ , whereas in all of the other models, stable hysteretic response without significant change in brace load carrying capacity is specified. In addition, small local undulations in the hysteretic curve of the models including the gap are captured because of local buckling of the core plate under compression. Fig. 8 shows the buckled shape of models  $S_{1g0.5}$ ,  $S_{5g2}$ , and  $S_{1g0}$  including the von Mises stress contours. The values of  $P_e/P_y$  are

calculated for all 13 BRB specimens and are given in Table 2. In addition, the factor  $\beta$  is calculated and shown in Table 2. Based on the results of the analysis, as shown in Table 2, models with a  $P_e/P_y$  ratio greater than 1.2 do not experience overall buckling during axial loading of up to a core strain of 2%. In addition, as shown in Table 2, these models experience a  $P_e/P_y$  ratio greater than  $\beta$ . Therefore, the analysis results confirm the validity of Eq. (7). In models  $S_{1g0}$  through  $S_{4g0}$ , with direct contact between the core and the BRM, local buckling of the core plate does not occur under incremental compression loading. Fig. 7 confirms this phenomenon. In addition, Fig. 7 shows that the local declines in hysteretic curve increases because of the increase in gap amplitude. In model  $S_{1g0}$  with a  $P_e/P_y$  ratio less than 1.2, the brace member causes lateral deflection as the compressive displacement increases and the lateral deflection rises. Contact forces acting on the upper side of the BRM increase and buckling of the brace member occurs when the moment at the center of the BRM reaches the yield moment of the BRM as a result of the contact forces. In models  $S_{1g0.5}$  and  $S_{5g2}$  including the gap and with a  $P_e/P_y$  ratio smaller than 1.2, the lateral deflection rises to the deformation of the higher order buckling modes. The contact forces acting on both sides of the restraining member increase under compression and cause global buckling of the brace. The results showed that the models with a  $P_e/P_y$  ratio greater than 1.2 do not experience global buckling, regardless of the size of gap. However, in the models with gaps, when  $P_e/P_y$  is greater than 1.2, severe inelastic excursions occur in the core plate under compression, which induces the lateral opening of the BRM member without overall buckling. Previous studies conducted by Tremblay et al. also confirm this phenomenon [10]. Therefore, providing a sufficient gap between the core plate and the BRM to accommodate lateral expansion of the core plate does not significantly affect the hysteretic response of the BRB if the BRM is stiff enough, i.e., if  $P_e/P_y \geq 1.2$ . In addition, the provided gap allows for free axial deformation of the core plate and reduces the amount of frictional forces at the interface. The results showed that the number of contact points between the BRM and the core plate gradually increases with more pronounced curvature. The buckles at large compression displacements are also more closely spaced at the core ends, as shown in Fig. 9b. The opening of the BRM attributable to higher order buckling of the core in models with adequate strength of BRM is shown in Fig. 9a in which the colors represent the von Mises stress contours in the encasing member indicating that the core imposes outward forces on the BRM that are resisted by the welds connecting the two upper and lower BRM components. The contact forces acting on the encasing wall cause minor bending in the BRM corresponding to the initial out of straightness. However, the BRM remains elastic while its rigidity is large enough. In the other words, while the rigidity of the encasing is large enough, total contact forces acting on upper and lower encasing walls are approximately balanced together and overall buckling does not occur.

Based on the results, the authors suggest an overall buckling prevention condition of BRBs where the suggested expression is  $P_e/P_y \geq 1.2$ . The results showed that the axial forces at the mid-point of the core plates in the models that buckle in compression are nearly  $1.2P_y$  at the onset of the brace global buckling. If the value of the  $P_y$  in the  $P_e/P_y$  ratio is substituted by  $1.2P_y$ , the use of the modified equation  $P_e/(1.2P_y) \geq 1$  or

Table 2  
Analysis results for the proposed BRBs.

ABAQUS results				
Model	$\alpha = P_e/P_y$	$\beta$	Brace global buckling	Core local buckling
<i>gap = 0 (direct contact)</i>				
$S_{1g0}$	1.09	1.11	Yes	No
$S_{2g0}$	1.49	1.13	No	No
$S_{3g0}$	1.98	1.15	No	No
$S_{4g0}$	2.53	1.15	No	No
<i>gap = 2.0 mm</i>				
$S_{1g2}$	1.29	1.24	No	Yes, opening of BRM
$S_{2g2}$	1.73	1.26	No	Yes, opening of BRM
$S_{3g2}$	2.21	1.30	No	Yes, opening of BRM
$S_{4g2}$	2.82	1.30	No	Yes, opening of BRM
$S_{5g2}$	1.10	1.25	Yes	Yes
<i>gap = 0.5 mm</i>				
$S_{1g0.5}$	1.13	1.15	Yes	Yes
$S_{2g0.5}$	1.54	1.16	No	Yes, opening of BRM
$S_{3g0.5}$	2.03	1.19	No	Yes, opening of BRM
$S_{4g0.5}$	2.60	1.19	No	Yes, opening of BRM

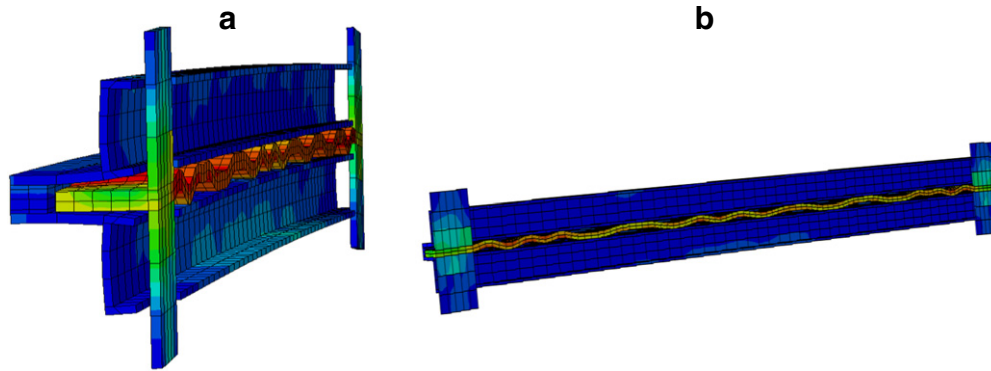


**Fig. 9.** a) Opening of the BRM in model  $S_{4g2}$ ; b) local buckling of the core in model  $S_{1g0}$ . (For interpretation of the references to color in this figure legend, the reader is referred to the web version of this article.)

$P_e/P_y \geq 1.2$  instead of the original equation  $P_e/P_y \geq 1$  proposed by Watanabe et al. [16] would be vindicated, and the results confirm its validity. However, a resistance factor of 0.85 may be included in the numerator for design purposes. Then, the above expression can be written as  $P_e/P_y \geq 1.4$ , which nearly coincides with the equation suggested by Powell, i.e.,  $P_e/P_y \geq 1.5$  [24].

The energy time history was computed during the analysis for all of the models. Fig. 10 shows the energy time histories for model  $S_{1g2}$ . The total work corresponds to the energy time histories fed into the system, and this energy is almost entirely dissipated through core plastic deformations. Fig. 10 represents the lower level energies of the system, the elastic strain energy, the energy dissipated by friction between the core and the BRM, and the energy dissipated by the artificial damping used for stabilization purposes. Elastic strain energy is stored in the system in each loading sequence. The higher peaks correspond to the compression displacement excursions because additional strain energy is induced in the BRM as the axial load is transferred into the BRM. Energy dissipation by friction occurs during the compression displacement excursions. The amount of dissipated energy increases as the imposed displacement and the contact forces increase. The energy associated with convergence stabilization increases steadily and represents on average 3% of the total energy input at the end of the analyses of all 13 models.

## 5. Conclusions

One of the underlying requirements of buckling restrained braces is the performance of avoiding overall buckling until the brace member reaches target displacement and sufficient ductility.

This required performance becomes important as the BRB is lightened and the strength and rigidity of the restraining member are reduced. A new generation of BRBs, called all-steel BRBs, is a class of BRBs with lighter buckling restraining components than conventional BRBs. In this family of BRBs, a light steel component is used as a restraining member instead of the mortar-filled tubes used in conventional BRBs, which may result in overall buckling of the brace caused by inadequate rigidity and strength of the restraining components. In this paper, the overall buckling prevention condition of all-steel BRBs is numerically examined by the finite element analysis method. Among the 13 BRB models, three models that had a  $P_e/P_y$  ratio of less than 1.2 experienced global buckling during cyclic loading of the brace of up to a core strain of 2%. In those buckled BRBs, the  $P_e/P_y$  ratios were less than factor  $\beta$  in Eq. (7), which confirms the validity of that equation, whereas in the other models, with a  $P_e/P_y$  ratio greater than 1.2, no buckling was captured in the compression. Therefore, the authors propose an overall buckling prevention condition of  $P_e/P_y \geq 1.2$  instead of the original equation suggested by Watanabe et al. [16]. However, this minimum  $P_e/P_y$  ratio is thought to be applied by exerting a safety factor of 0.85. Thus, a ratio of  $P_e/P_y \geq 1.4$  might be used for design purposes. In addition, results showed that providing a gap between the core and the BRM, despite some local instability attributable to higher mode buckling of the core, would not significantly affect the hysteretic behavior of the brace, if the strength and rigidity of the BRM are sufficient, i.e.,  $P_e/P_y \geq 1.2$ . Further experimental and analytical investigations are necessary to examine the overall buckling prevention condition of BRBs considering different gap sizes, different BRM types, and frictional response effects in all-steel buckling restrained braces.

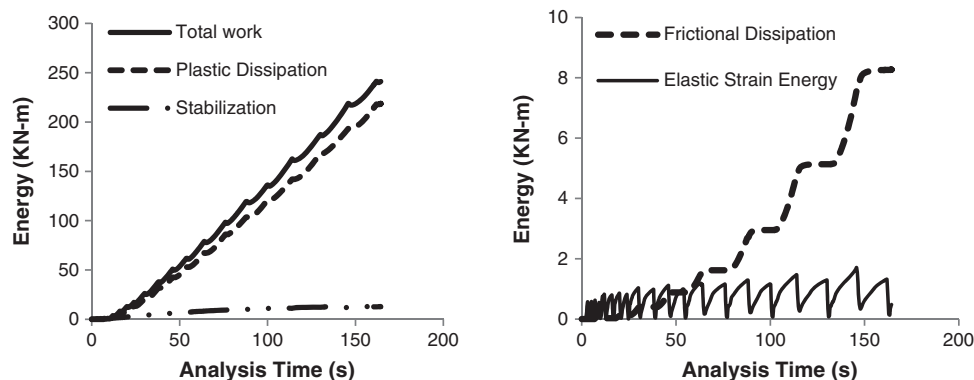


**Fig. 10.** Energy time histories in the numerical model of  $S_{1g2}$ .

## References

- [1] Black CJ, Makris N, Aiken ID. Component Testing, stability analysis, and characterization of buckling restrained braced braces. Report No. PEER 2002/08, Univ. of California, Berkeley, CA.
- [2] Inoue K, Sawaizumi S, Higashibata Y. Stiffening requirements for unbonded braces encased in concrete panels. *ASCE J Struct Eng* 2001;127(6):712–9.
- [3] Qiang X. State of the art of buckling-restrained braces in Asia. *J Constr Steel Res* 2005;61:727–48.
- [4] Clark P, Aiken I, Kasai K, Ko E, Kimura I. Design procedures for buildings incorporating hysteretic damping devices. Proc., 69th annual convention. SEAOC; 1999. p. 355–71.
- [5] Sabelli R, Mahin S, Chang C. Seismic demands on steel braced frame buildings with buckling-restrained braces. *Eng Struct* 2003;5:655–66.
- [6] Fahnestock LA, Sause R, Ricles JM. Seismic response and performance of buckling-restrained braced frames. *J Struct Eng* 2007;133(9):1195–204.
- [7] Takeuchi T, Suzuki K, Marukawa T, Kimura Y, Ogawa T, Sugiyama T, et al. Performance of compressive tube members with buckling restrained composed of mortar in-filled steel tube. *J Struct Constr Eng* 2005;590:71–8.
- [8] Tembata H, Koetaka Y, Inoue K. Out-of-plane buckling load of buckling restrained braces including brace joints. *J Struct Constr Eng* 2004;581:127–34.
- [9] Kinoshita T, Koetaka Y, Inoue K, Iitani K. Criteria of buckling-restrained braces to prevent out-of-plane buckling. *J Struct Constr Eng* 2007;621:141–8.
- [10] Tremblay R, Bolduc P, Neville R, DeVall R. Seismic testing and performance of buckling restrained bracing systems. *Can J Civ Eng* 2006;33(1):183–98.
- [11] Kato M, Usami T, Kasai A. A numerical study on cyclic elasto-plastic behavior of buckling-restraining brace members. *JSCE J Struct Eng* 2002;48A:641–8.
- [12] Watanabe N, Kato M, Usami T, Kasai A. Experimental study on cyclic elasto-plastic behavior of buckling-restraining braces. *JSCE J Earthquake Eng* 2003;27 [Paper No. 133].
- [13] Usami T. Guidelines for seismic and damage control design of steel bridges. Edited by Japan Society of Steel Construction 2006; Gihodo-Shuppan, Tokyo [in Japanese].
- [14] Eryasar M, Topkaya C. An experimental study on steel-encased buckling restrained brace hysteretic damper. *J Earthquake Eng Struct Dyn* 2010;39:561–81.
- [15] AISC (American Institute of Steel Construction). Seismic provisions for structural steel buildings, Chicago, IL; 2010.
- [16] Watanabe A, Hitomi Y, Yaeki E, Wada A, Fujimoto M. Properties of braces encased in buckling-restraining concrete and steel tube. Proceedings of 9th world conference on earthquake engineering; 1988. p. 719\_24.
- [17] Iwata M, Murai M. Buckling-restrained brace using steel mortar planks: performance evaluations a hysteretic damper. *Earthq Eng Struct Dyn* 2006;35:1807–26.
- [18] Matsui R, Takeuchi T, Hajjar JF, Nishimoto K, Aiken I. Local buckling restraint condition for core plates in buckling-restrained braces. Proc. 14th World Conf. on Earthquake Eng; 2008. Beijing, China, Paper No.05-05-0055.
- [19] Korzekwa A, Tremblay R. Numerical simulation of the cyclic inelastic behavior of buckling restrained braces. London: Taylor & Francis Group978-0-415-56326-0; 2009.
- [20] Fujimoto M, Wada A, Saeki E, Watanabe A, Hitomi Y. A study on the unbonded brace encased in buckling restraining concrete and steel tube. *J Struct Constr Eng* 1988;34B:249–58 [in Japanese].
- [21] ABAQUS. Standard user's manual version 6.3. Pawtucket, RI: Hibbitt, Karlsson & Sorensen, Inc.; 2003.
- [22] Chou C, Chen S. Sub-assembly tests and finite element analyses of sandwiched buckling restrained braces. *Eng Struct* 2010;32:2108–21.
- [23] Usami T, Ge H, Luo X. Experimental and analytical study on high-performance buckling restrained brace dampers for bridge engineering. Proceeding of 3rd International Conference on Advances in Experimental Structural Engineering, October 15–16; 2009. San Francisco.
- [24] Powell S. Personal communication, Star Seismic LLC 2002. Park City, UT.